Effects of atmospheric circulations on the interannual variation in $PM_{2.5}$ concentrations over the Beijing-Tianjin-Hebei region in 2013-2018

Xiaoyan Wang*[1,2], Renhe Zhang[1,2]

1. Department of Atmospheric and Oceanic Sciences & Institute of Atmospheric Sciences, Fudan University, Shanghai, China
2. Big Data Institute for Carbon Emission and Environmental Pollution, Fudan University, Shanghai, China

Correspondence to: wangxyfd@fudan.edu.cn

Submitted to Atmospheric Chemistry and Physics

Abstract

The Chinese government has made many efforts to mitigate fine particulate matter pollution in recent years by taking strict measures on air pollutants reduction, which has generated the nationwide improvements in air quality since 2013. However, under the stringent air pollution controls, how the wintertime $PM_{2.5}$ concentration (i.e., the mass concentration of atmospheric particles with diameters less than 2.5 μm) varies and how much the meteorological conditions contribute to the interannual variations in $PM_{2.5}$ concentrations are still unclear, which is very important for the local government to assess the emission reduction of previous year and adjust mitigation strategies of next year. The effects of atmospheric circulation on the interannual variation

in wintertime $PM_{2.5}$ concentrations over the Beijing-Tianjin-Hebei (BTH) region in the period of 2013-2018 are evaluated in this study. Generally, the transport of clean and dry air masses and unstable boundary layer working with the effective near-surface horizontal divergence or pumping action at the top of the boundary layer benefit for the horizontal or vertical diffusion of surface air pollutants. Instead, the co-occurrence of a stable boundary layer, frequent air stagnation, positive water vapor advection and deep near-surface horizontal convergence exacerbate the wintertime air pollution. Favorable circulation conditions lasting for 2~4 days are beneficial for the diffusion of air pollutants, and 3~7 days of unfavorable circulation events exacerbate the accumulation of air pollutants. The occurrence frequency of favorable circulation events is consistent with the interannual variation in seasonal mean $PM_{2.5}$ concentrations. There is better diffusion ability in the winters of 2014 and 2017 than in other years. A 59.9% of the observed decrease in $PM_{2.5}$ concentrations in 2017 over the BTH region could be attributed to the improvement in atmospheric diffusion conditions. It is essential to exclude the contribution of meteorological conditions to the variation in interannual air pollutants when making a quantitative evaluation of emission reduction measurements.

Introduction

Rapid economic development and associated emissions have led to recent severe air pollution over China, which has become a central issue of concern for the public and governments (Mu and Zhang, 2014;Song et al., 2018;Tao et al., 2018;Wang et al., 2018;Wang et al., 2015;Zhang et al., 2014;Zhao and Garrett, 2015).. High levels of fine particulate matter ($PM_{2.5}$) concentrations influence people's daily lives and threaten public health (Liu et al., 2019;Zhao et al., 2018a;Hong et al., 2019;Zhang et al., 2017;Hu et al., 2019). In addition, they are efficient in scattering and absorbing solar radiation, and are involved in the climate change by changing the surface energy budget (Bi et al., 2016;Chen et al., 2019b;Che et al., 2019;Feng and Wang, 2019;He et al., 2018b;Li et al., 2018;Jian et al., 2018;Wang et al., 2009;Wang et al., 2017;Yang et al., 2018;Zhao et al., 2019c). To mitigate $PM_{2.5}$ pollution, the Chinese government issued the Air Pollution Prevention and Control Action Plan (hereinafter referred to as the Clean Air Action hereinafter) in 2013, which required the Beijing-Tianjin-Hebei

(BTH) region, Yangtze River Delta and Pearl River Delta to reduce their $PM_{2.5}$ concentrations by 15~25% from 2013 to 2017 (China's State Council, 2013). A series of stringent clean air actions was implemented to improve air quality, including improving industrial emission standards, phasing out small and polluting factories, strengthening vehicle emission standards and more (Zhao et al., 2019b;Zhang and Geng, 2019). To further improve air quality, the state council has released a three-year action to win the battle for a blue sky in 2018, solidifying a timetable and roadmap for improving air quality. By 2020, emissions of sulfur dioxide and nitrogen oxides are required to decline by at least 15% from 2015 levels, while cities with low air quality standards should see their $PM_{2.5}$ density fall by at least 18%, according to the plan (China's State Council, 2018). To achieve these goals, many efforts have focused on adjustments to industrial, energy and transportation structures involved with central to local government.

With the implementation of the toughest-ever clean air actions from Clean Air Action, the anthropogenic emissions show significant decreased by 59% for SO_2, 21% for NOx, 23% for CO, 36% for PM_{10} and 33% for primary $PM_{2.5}$ from 2013 to 2017 (Zheng et al., 2018;Wang et al., 2019b;Zhang et al., 2020). As a consequence, air quality in China improved significantly in terms of annual mean $PM_{2.5}$ concentrations, polluted days and pollution durations from 2013 to 2017, and surpassed the mitigation targets of the Clean Air Action (Fan et al., 2020;Gui et al., 2019;Zhao et al., 2018c;Zhong et al., 2018;Zhang et al., 2019a). By the end of 2017, the BTH region achieved its primary goal of reducing the annual average $PM_{2.5}$ concentration to less than 60 $\mu g/m^3$ with a decreasing trend of -9.3±1.8 $\mu g/m^3$ (Wang et al., 2019b). However, in addition to air pollutants emissions, atmospheric meteorological conditions play an important role in the long-range transport, accumulation, vertical diffusion, scavenging and chemical production of particles, which drives the evolution of every air pollution episode (Leung et al., 2018;Huang et al., 2018;Sun et al., 2019;Garrett et al., 2010;Wang et al., 2016;Wang and Wang, 2016;Zhang et al., 2012;Zhao et al., 2018b). Moreover, the interannual to interdecadal variations in meteorological or climate signals (e.g., monsoon intensity, variation in sea ice, and the occurrence of El Niño Southern Oscillation (ENSO) and North Atlantic Oscillation (NAO)) also have significant effects on the variation in ambient $PM_{2.5}$ concentrations (Chen et al., 2019a;Chen and Wang, 2015;Dang and Liao, 2019;Feng et al., 2019;Li et al., 2016;Yin et al., 2019;Yin et al., 2017;Zhao et al., 2018d;Chen et al., 2019c).

The global warming associated with climate change may also contribute to the air pollution in China (Cai et al., 2017; Zhang, 2017).

Recently, many researchers investigated how much of the recent decreased $PM_{2.5}$ concentrations could be attributed to the contribution from emission reduction compared to the effects of atmospheric elements. The studies have been carried out to evaluate the relative effects of emission reduction and meteorological conditions on the recent decrease in $PM_{2.5}$ concentrations (Ding et al., 2019;Guo et al., 2019;He et al., 2018a;Zhang et al., 2019d;Zhao et al., 2019a). Based on a multiple linear regression model, 12% of the decreased $PM_{2.5}$ over China is due to favorable meteorological conditions between 2013 and 2018 (Zhai et al., 2019). For the BTH region, Zhang et al. (2019c) used the parameter linking air quality and meteorology (PLAM) index (a meteorological pollution index for air quality) to evaluate meteorological conditions, and found that only approximately 5% of the 39.6% reduction in $PM_{2.5}$ in 2017 could be attributed to meteorological changes. The relative contribution of emission reduction to the decreased $PM_{2.5}$ concentrations in Beijing calculated by the statistical model and Weather Research and Forecasting-Community Multiscale Air Quality (WRF-CMAQ) was 80%, indicating that emission reductions were crucial for air quality improvement in Beijing from 2013 to 2017 (Chen et al., 2019d). In addition, Zhang et al. (2019b) quantified the contribution of different emission control policies to the rapid improvement in $PM_{2.5}$ pollution over China from 2013 to 2017 and highlighted the significant effects of strengthening industrial emission standards and upgrading industrial boilers on air quality improvement during the Clean Air Action.

Based on the investigation of different methods, the effectiveness of emission mitigation actions was confirmed to drive the recent remarkable improvement in air quality in China since 2013. However, most of the existing studies have focused on the relative long-term variation of air quality (i.e., five to six years since 2013) and evaluated emission reduction effects over a multiyear time scale. The Chinese government took a series of steps to reduce air pollutant emissions, which requires a certain sacrifice regarding economic growth. In this situation, the local government need an accurate evaluation of the emission reduction effects during the previous year and reasonable adjustment of the mitigation policies of next year to keep the balance of economic growth and

environmental protection. The accurate evaluation of emission reduction effects should exclude the meteorological element contribution to the interannual variations of air quality. China's air quality shows obvious seasonal and regional distributions, with more frequent severe air pollution episodes in winter time and higher air pollutant concentrations in eastern China. As one of the three key regions in the Clean Air Action, lots of mitigation measurements have been taken over BTH region in recent years, which results in the significant improvement of local air quality, especially in winter time. But the relative contribution from meteorological factors are still unclear. Therefore, the contribution of meteorological conditions to the interannual variation in wintertime $PM_{2.5}$ concentrations over the BTH region will be discussed in this study.

2. Data and Methods

2.1 On-site $PM_{2.5}$ mass concentration

The wintertime (December to February of the following year) hourly observed $PM_{2.5}$ mass concentration dataset over China from 2013 to 2018 was provided by the Ministry of Ecology and Environment of the People's Republic of China (http://106.37.208.233:20035). This study mainly focuses on the region of BTH region (113.5º-119ºE and 36º-42.5ºN, the solid-line box in Fig. 2), and 114 $PM_{2.5}$ stations are available over this region. Daily $PM_{2.5}$ data is set as missing when the valid hourly data on the specific day is less than 40%.

2.2 Method of atmospheric circulation classification

Commonly used objective classification methods include correlation, clustering, nonlinear methods, principal component analysis (PCA), and fuzzy analysis. Huth et al. (2008) compared these five classification methods and proposed that the performance of the T-mode PCA was the best in terms of its reproduction of predefined types, temporal and spatial stabilities, and reduced dependence on preset parameters. In this model, the input data matrix is space-time two-dimensional: the rows represent spatial grids, and the columns is time series. The data are divided into ten subsets to speed up computations, and the principal components (PCs) are achieved using the singular value

decomposition for each subset and an oblique rotation is applied to the PCs to achieve better classification effects. Then, chi-square test is used to evaluate the ten classifications based on the subsets and the subset with the highest sum is chosen and assigned to a type. The T-mode PCA has been successfully applied to studies of general circulation models (Huth, 2000), climate change (Cavazos, 2000), and local air pollution (Xu et al., 2016; Valverde et al., 2015; Miao et al., 2017; Li et al., 2019). Zhang et al. (2012) first employed the obliquely rotated T-mode PCA method developed by European Cooperation in Science & Technology (COST) action 733 (http://www.cost733.org) (Philipp et al., 2014) to identify the circulation pattern that is conductive to particulate matter pollution in North China. In this study, the four-times-daily dataset of the fifth generation European Centre for Medium-Range Weather Forecasts (ECMWF ERA5) atmospheric reanalysis in winters from 2013 to 2018 with a horizontal resolution of 0.25º was used for synoptic circulation classification. The daily mean geopotential height fields at 925, 850 and 500 hPa were applied to the T-mode PCA method in the Cost733 toolbox. Our target region is 105º-125ºE and 30º-55ºN (the dashed box in Fig. 3). Prior to using Cost733, the number of principal components need to be defined manually. To exclude the influences of various number of principal components, sensitivity tests with principal components from 2 to 10 are conducted in this study, the explained variances of which are shown in Fig. S1.

2.3 Model simulation

The regional chemical/transport model WRF chemical model (WRF-Chem) version 4.0, was applied to simulate the effects of meteorological condition variation on seasonal air pollution over northern China at a horizontal resolution of 9 km (245*220 horizontal grid cells) and vertical resolution of 33 layers. The simulation domain covers most areas of the North China region (Fig. 10). The initial and lateral meteorological boundary conditions are derived from the National Centers for Environmental Prediction Final (NCEP FNL) reanalysis data every 6 hours. The chemical and aerosol mechanisms used were the RADM2 chemical mechanism from Stockwell et al. (1990) and MADE/SORGAM aerosols (Ackermann et al., 1998; Schell et al., 2001). MADE/SORGAM are used to simulate all major aerosol components including sulfate, nitrate, ammonium, black carbon, organic carbon, sodium, chloride, mineral dust, and water content.

Madronich photolysis was used to calculate photochemical reactions. Other major physical processes included the CAM shortwave radiation (Collins et al., 2004), RRTMG longwave radiation (Iacono et al., 2008), the unified Noah land-surface model land surface option and MYJ planetary boundary layer parameterization (Janjić, 1994). To consider the couple effects of aerosol and meteorology, the parameterization of feedback from aerosol to radiation, feedback from convection to atmospheric radiation and photolysis, wet scavenging and cloud chemistry are turned on in the simulation.

To evaluate the impacts of meteorological contributions on the $PM_{2.5}$ variation between the 2016 winter (Dec. 2016 to Feb. 2017) and 2017 winter (Dec. 2017 to Feb. 2018) over the BTH region, we conducted two sensitivity runs: the same emissions as the 2016 winter and the actual meteorological conditions of 2016 and 2017. Thus, the difference in the simulated $PM_{2.5}$ concentrations between the 2016 and 2017 winters could be attributed to the meteorological variation, which can be assumed as a typical value of meteorological contribution to the interannual variation of PM2.5 concentrations. The anthropogenic emission inventory for 2016 developed by Tsinghua University was used in this study (available at http//www.meicmodel.org), as is named the Multiresolution Emission Inventory for China (MEIC), containing monthly anthropogenic emissions of SO2, NOx, CO, NH3, $PM_{2.5}$, PMcoarse, BC, OC and NMVOCs. The horizontal resolution of the MEIC used in this study is 0.25°. Each simulation is initialized at 00:00 UTC on Nov. 23, and the first week simulations are regarded as the spin-up period. Daily mean $PM_{2.5}$ concentrations between Dec. 1, 2016 to Feb. 28, 2017, and Dec. 1, 2017 to Feb. 28, 2018, are used to investigate the effects of meteorological conditions on seasonal air pollution.

3. Results

3.1 Dominant synoptic circulation types in winter over the BTH region

As shown in Fig.1, the wintertime $PM_{2.5}$ concentrations over the BTH region show a remarkable decrease from 2013 to 2018 due to a series of air pollution reduction measures. Compared to 2013, the mean $PM_{2.5}$ concentration for 2018 decreased by 35.6% over 114 stations around the BTH region

(cf. Table 1). However, under the background of improved air quality, evident interannual variations in $PM_{2.5}$ concentrations have been observed in recent years. The $PM_{2.5}$ concentrations in the winters of 2016 and 2018 are higher than those in the same period of the previous year, with mean values increasing by 18% and 13.36%, respectively. The high emissions of primary fine particulate matters and its precursors are considered as internal factors of severe $PM_{2.5}$ pollution in China; thus, emission reduction is the most direct and effective way to improve local air quality. However, the evolution of each air pollution episode is strongly affected by the local synoptic circulation pattern. Both emissions and atmospheric conditions are related to the ambient $PM_{2.5}$ concentration level. It is essential to exclude the atmospheric circulation impacts on air quality when assessing emission mitigation effects.

We use synoptic circulation types to measure the ability of atmospheric circulation to accumulate, remove, and transport air pollutants. The daily mean geopotential height fields at 925, 800 and 500 hPa in the winters of 2013 to 2018 (total of 451 days) are used to conduct objective synoptic circulation classification based on the T-mode PCA method with the Cost733 toolbox. Three levels of geopotential height fields (i.e., 925 850 and 500 hPa) in the lower to middle troposphere over 105º-125ºE and 30º-55ºN are used in circulation type (CT) classification. Six typical synoptic circulation types (CTs) are identified during winter in the BTH region, with a total explained variance of 70% (Fig. S1). The horizontal (i.e., sea level pressure (SLP), wind, relative humidity (RH) and boundary layer height (BLH)) and vertical (i.e., atmospheric stability, vertical velocity, temperature and divergence) distributions of meteorological variables are used to illustrate the mechanism behind CT effects on air pollution. To obtain a broad view of the six CTs, the horizontal distribution of atmospheric circulation patterns, as shown in Fig. 2 and Fig. 3 cover a larger area than the area used in the CT classification with the Cost733 toolbox.

Fig. 2 and Fig. 3 exhibit the original and anomalous patterns of the mean SLP and surface wind field of each CT, respectively. CT1 is the most frequent CT during the study period with an occurrence frequency of 33% based on the results of the Cost733 classification. CT1 shows that a high-pressure system originates in the Siberian region extending along central Inner Mongolia to southern China. Northwesterly winds prevail in northern China and turn into northerly winds in southern China. The

mean wind speed is 3.27 m/s over the BTH region (cf. Table 2), which is the highest among the six CTs and benefits the outward transport of local air pollutants. Fig. 3 shows the SLP and surface wind anomalies of each CT. In the CT1 situation, the BTH region is located west of the cyclonic anomaly, which is dominated by an obvious northwesterly wind anomaly. The wind field pattern corresponds to the negative RH anomaly over the BTH region in Fig. 4. The vertical profiles of dynamic and thermodynamic stratification are included to investigate vertical diffusion. Based on the vertical distribution of atmospheric stability shown in Fig. 5, atmospheric stratification is characterized by a stable layer at the top of the boundary layer for all the cases. For CT1, an obvious unstable stratification occurs at the bottom of boundary layer over the BTH region, which enhances the turbulent activities and is beneficial for the vertical diffusion of air pollutants. The unstable boundary layer is also confirmed by the positive BLH anomaly and elevated negative temperature anomaly, as shown in Fig. S2 and Fig. S3. Fig. S4 shows a strong surface divergence and strong top convergence vertical pattern in CT1, which generates sinking movement over the BTH region. As shown in Fig. 6, a subsidence anomaly appears at the lower to middle troposphere over the BTH region with a mean descending velocity of 0.04 pa/s between 850 and 1000 hPa. The strong downdraft brings a clean and dry air mass to the surface and increases the horizontal divergence of surface air pollutants (shown in Fig. S4). The cold, clean and dry air mass transported by the surface northwesterly winds, unstable boundary layer and strong horizontal divergence are favorable for the improvement in ambient air quality.

The occurrence frequency of CT2 is 11%. As shown in Fig. 2, a high-pressure system around Baikal is obvious under the CT2 condition, which is stronger and further east than CT1. The BTH region is located at the ridge of the high-pressure system with weak northwesterly winds occurring in the northern BTH region, which turn to northeasterly in the southern BTH region. The anomalous fields in Fig. 3 show a large area of a positive SLP anomaly over the north of 40ºN. The BTH region is just located at the south edge of the anticyclone anomaly with prevailing northeasterly surface wind. Fig. 4 shows a weak negative RH anomaly over the BTH region due to the dry wind from the northeast. Similar to CT1, CT2 also shows an unstable stratification in the boundary layer, which increases the vertical diffusion of air pollution. Both the weak positive BLH anomaly and elevated negative temperature anomaly indicate the enhanced instability of the atmospheric boundary layer

(Figs. S2-S3). Intense updraft is stimulated by strong convergence at the surface working with strong divergence at the top of the boundary layer, as shown in Fig. S4. As shown in Fig. 6, upward movement dominates in the middle-low troposphere over the BTH region with a mean ascending velocity of 0.0358 pa/s between 850 and 1000 hPa. Although the elevated temperature stability is relatively strong in CT2, the bottom-up updraft breaks through the stable layer and brings the surface air pollutants to the free atmosphere. In summary, the unstable boundary layer working with the upper divergence pumping action enhances the vertical diffusion of surface air pollutants, which will decrease the surface concentrations of air pollutant.

CT3 shows a relatively uniform SLP distribution with a weak pressure gradient over the BTH region as shown in Fig. 2. The prevailing westerly wind hinders the southward transport of the cold air mass to some extent. The cyclonic anomaly with southwesterly wind can be found over the BTH region. As shown in Fig. 3, the southwesterly wind transports the upstream air pollutants and warm moisture to the BTH, which accelerates the hygroscopic growth of particles, promotes the gas-to-particle transformation and increases the local air pollutant concentration (Wang et al., 2019a). The positive RH and temperature anomaly in Fig. 4 and Fig. S3 correspond to the southwesterly wind anomaly. Unlike to CT1 and CT2, CT3 shows a stable stratification below 700 hPa. In addition, the upper unstable stratification of CT3 is lower than that of CT1 and CT2, indicating a negative BLH anomaly (as shown in Fig. S2). CT3 also shows upward movement over the BTH region, but it is weaker than CT2 by one order of magnitude. By contrast, the effects of the stronger near-surface convergence will offset the upward transport, which will increase the local air pollutants. The stable boundary layer, southeasterly warm moisture and effective convergence aggravate local air pollution.

For the cases of CT4 and CT5, the BTH region is co-located with a weak surface anticyclone with low average surface winds of 2.24 and 2.58 m/s, respectively. The calm surface winds coexisting with the lower BLHs (cf. Fig. S2) decrease the ventilation coefficient and increase the occurrence of air stagnation conditions. The surface anomaly fields show southeasterly and southerly winds in CT4 and CT5, respectively. As shown in Fig. 4, the northward wind anomaly increases the humidity and air pollutants of the BTH region. Based on the vertical profiles of temperature and atmospheric

stability, an elevated positive temperature anomaly increases the stability of the boundary layer, thus reducing the vertical diffusion of air pollutants. The weak near surface convergence could increase the accumulation of air pollution, but moderate upward movement will bring the surface air pollutants to the outside of the boundary layer, which offsets the surface convergence to some extent. CT4 and CT5 had the same occurrence of 15% during the study period. Although the CT4 and CT5 show different large-scale surface circulation patterns, the meteorological variables over the BTH region are almost the same. The air stagnation conditions and southerly water vapor transport result in the accumulation and hygroscopic growth of particles.

In terms of CT6, the BTH region is located at the ridge of the Mongolian anticyclone, and its high-pressure system is weaker than that of CT2. The prevailing wind turns from northwest to northeast over the BTH region. As shown by the surface meteorological anomaly distribution, the BTH region is situated at the border between the northern anticyclonic and southern cyclonic anomalies with prevailing northeasterly wind coming from the Bohai Sea. A large amount of water vapor from the sea plays an important role in the hygroscopic growth of particles over the BTH region. Fig. 5 indicates a stable boundary layer when CT6 occurs, which reduces the vertical diffusion of surface air pollutants. CT6 shows a deep horizontal convergence under 850 hPa, which is favorable for the accumulation of moisture and air pollutants. The effect of the relatively weak divergence above strong convergence is not distinct for the improvement in surface air quality. Therefore, the circulation pattern of warm moist flow from the sea, a stable boundary and effective horizontal convergence exacerbates local air pollution.

3.2 Atmospheric circulation pattern effects on air quality

The potential mechanisms of the CT effects on local air quality are discussed in section 3.1. Combinations of the following situations are favorable for the improvement in air quality: transport of a clean and dry air mass, unstable boundary layer, effective horizontal divergence and vertical transport of air pollutants to the free atmosphere. In contrast, the positive humidity anomaly, stable boundary layer, frequent air stagnation conditions and deep horizontal convergence exacerbate air pollution.

To exclude the effects of interannual variation in air quality due to the emission reduction background, the daily $PM_{2.5}$ concentration distribution displayed by year and CT, as shown in Fig. 7 reveals the effects of CT on air quality. The mean and median values of $PM_{2.5}$ concentrations during each CT are summarized in Table 1. The mean and median $PM_{2.5}$ concentrations in the CT1 condition are both lower than the seasonal mean and median for all years. Under the CT2 condition, the $PM_{2.5}$ concentrations are also lower than the seasonal mean except for 2014. However, the $PM_{2.5}$ concentrations are generally higher than the seasonal mean in CT3-CT6. As for the multiyear average, it shows distinctly lower $PM_{2.5}$ concentrations in CT1 and CT2 than the other CTs. Based on the $PM_{2.5}$ concentration in each CT, CT1 and CT2 can be considered as favorable CTs for air quality, which are beneficial for the diffusion of air pollutants, and CT3-CT6 are unfavorable CTs, which exacerbate air pollution.

Giving the above analysis, $PM_{2.5}$ concentration tended to be lower than normal when a favorable CT occurred, and vice versa. Therefore, the occurrence frequency of each CT plays an important role in air quality during the study period. CT1 and CT2 are combined as the favorable circulation, and CT3-CT6 are referred to as the unfavorable circulation. Fig. S5 exhibits the seasonal occurrences of favorable and unfavorable circulation types. Fifty-four days of unfavorable circulation occurred in winter 2013, which is the greatest frequency during the study period. A higher unfavorable circulation frequency was also shown in 2014 and 2018 winters. In contrast, the favorable circulations were much higher in 2015 and 2017 winters than in the other winters. The seasonal frequencies of favorable and unfavorable circulations are in line with the trend in seasonal $PM_{2.5}$ concentrations. It is worth noting that although the seasonal mean $PM_{2.5}$ concentration in the winter of 2015 (Dec. 2015 to Feb. 2016) is lower than that of 2014, the $PM_{2.5}$ concentration in Dec. 2015 is much higher than that in Dec. 2014. The high $PM_{2.5}$ concentration in Dec. 2015 is consistent with the high frequency of unfavorable CTs during that time, which indicates the robustness of circulation classification.

However, every air pollution event has a duration from the development to decay stage. Generally, several days are needed for the accumulation of air pollutants, followed by a relatively quick removal. The variation in meteorological conditions controls the evolution of each air pollution

episode. Therefore, the duration of each CT determines the duration of the air pollution event. Fig. 8 exhibits the variation in the $PM_{2.5}$ concentration anomaly with the duration of favorable and unfavorable CTs. As discussed above, the favorable circulations generally correspond to the negative $PM_{2.5}$ concentration anomaly (lower than the monthly mean), while the unfavorable circulations result in a positive $PM_{2.5}$ concentration anomaly. When the favorable circulation duration is shorter than 4 days, the absolute values of the negative anomaly of $PM_{2.5}$ concentrations increase with the duration of favorable circulation; however, with the continuous increase in favorable circulation durations, the magnitude of the negative anomaly of $PM_{2.5}$ concentrations slightly decreases and remains unchanged. Similarly, the positive anomalies of the $PM_{2.5}$ concentrations increase with the duration of unfavorable circulation durations when the duration is less than 7 days. However, the effect of circulation on air pollutant diffusion is not obvious when a one-day favorable or one-two-day unfavorable circulation occurs. That is favorable CTs lasting 2~4 days are beneficial for the diffusion of air pollutants; and unfavorable circulation events lasting 3~7 days exacerbate the accumulation of air pollutants.

The occurrences of 2~4 days favorable circulation and 3~7 days of unfavorable CTs are shown in Fig. 9. It shows a high frequency of 2~4 days of favorable circulation in 2017 and 2014 with totally 15 and 13 days, respectively. The favorable circulation occurrences are lower in the winters of 2016 and 2018 than in the other winters. In terms of the 3~7 days of unfavorable circulations, the years of 2013, 2016 and 2018 show higher frequencies than the other years. Therefore, based on the occurrence of favorable and unfavorable CTs, the atmospheric diffusion abilities are better in 2014 and 2017 than in the other years. The significant improvement in air quality in 2014 and 2017 is consistent with the improvement in atmospheric diffusion abilities compared to their previous years.

3.3 Contributions of atmospheric diffusion condition variations to the $PM_{2.5}$ concentration decrease between 2016 and 2017

Although the interannual variation in $PM_{2.5}$ concentrations show good correlation with the occurrence of favorable or unfavorable circulation, Sec. 3.2 is just a qualitative analysis. Taking the interannual variation in $PM_{2.5}$ concentrations between 2016 and 2017 as an example, the model simulation based on the WRF-Chem model is used to evaluate the quantitative contributions of

meteorological condition variations to the $PM_{2.5}$ concentration decrease in 2017. The emissions are fixed in 2016 (Dec. 2016 to Feb. 2017), and the meteorological fields come from the NECP GDAS Final Analysis dataset for the 2016 and 2017 winters, respectively. The meteorological fields and air pollutants over some cities from north to south in the simulated domain (i.e., Shijiazhuang, Beijing, Tianjin, Xuzhou and Shanghai) are included to evaluate the performance of the model simulation. Fig. S6 shows the variations in the observed and simulated daily mean air temperature, sea level pressure, relative humidity and surface wind speed from Jan. to Feb. of 2017. Although the model slightly overestimates the surface wind speed over Shijiazhuang and Shanghai, most of the simulated meteorological variables agree well with the observations over all cities. For the concentration of air pollutants in Fig. S7, the model generally underestimates the $PM_{2.5}$ concentrations under highly polluted conditions, with a bias of 44.9%~59.6% (different cities) when the observed $PM_{2.5}$ was higher than 75 $\mu g/m^3$. However, the bias between the simulated and observed $PM_{2.5}$ concentrations decreased to 12.4%~26.8% at lower $PM_{2.5}$ concentration level. Due to the deficiency of the PBL scheme (Tie et al., 2015), the heterogeneous/aqueous process in the model (Li et al., 2011) and uncertainty in the emission inventory, current air quality models show limited capacity in severe air pollution episodes. However, the day-to-day variation in all the air pollutants can be well captured by the WRF-Chem model, with the highest correlation coefficient of 0.76 between the observed and simulated $PM_{2.5}$ in Xuzhou. Overall, both the meteorological variables and air pollutants are well reproduced by the WRF-Chem model, which provides confidence for further discussions.

The simulated seasonal mean $PM_{2.5}$ concentrations of the 2016 and 2017 winters are presented in Fig. S8. It shows a significant spatial distribution of seasonal $PM_{2.5}$ concentrations with higher concentrations over the BTH region, Shandong and Henan Provinces. Even though the emissions were set to the level of 2016, the simulated seasonal $PM_{2.5}$ concentrations in 2016 were much higher than those in 2017 due to the difference in meteorological fields. Fig. 10 exhibits the observed and simulated $PM_{2.5}$ concentration differences between 2017 and 2016. Both the observations and simulations show significant negative growth in $PM_{2.5}$ concentrations over northern China from 2016 to 2017 in winter but relatively weak positive growth over the lower Yangtze River Delta. The BTH region is located at the center of negative growth, with an observed 47.7 $\mu g/m^3$ decrease in

$PM_{2.5}$ concentration from 2016 to 2017 at 114 stations over the region of 113º-117.5ºE and 36º-42ºN. While, the simulated difference of $PM_{2.5}$ at these 114 stations is -11.7 μg/m^3, which is much lower than the observed value. The absolute $PM_{2.5}$ concentration would be underestimated because of the limited performance of the WRF-Chem model under severe air pollution; therefore, the relative differences between 2016 and 2017 are involved to evaluate the effects of meteorological field variations on the decrease in $PM_{2.5}$ concentrations. Based on the relative difference in $PM_{2.5}$ concentration between 2016 and 2017, the observed difference at the 114 stations over the BTH region is -37.7% compared to the mean value of 2016 winter, and the averaged simulated difference is -22.6%, which is due to the difference in meteorological conditions. Thus, 59.9% of the observed 37.7% decrease in $PM_{2.5}$ concentration in 2017 over the BTH region could be attributed to the improvement in atmospheric diffusion conditions. The variation of meteorological conditions plays an important role in the interannual variation in air pollutant concentrations.

4. Conclusions and Discussion

Recent severe $PM_{2.5}$ pollution in China has aroused unprecedented public concern. The Chinese government has implemented many emission reduction measurements, which has greatly improved the air quality recently. The wintertime $PM_{2.5}$ concentration of 2018 decreased by 35.6% compared to 2013 over the BTH region. However, there was obvious interannual variation in $PM_{2.5}$ concentrations from 2013 to 2018. Atmospheric circulation classification method based on the Cost733 toolbox is used to investigate the mechanism behind atmospheric circulation effects on air pollutant diffusion. Six CTs are identified during the winters from 2013 to 2018 over northern China, and two of which are considered as favorable circulations for air pollutant diffusion and the other four CTs exacerbate local air pollution. Generally, the transport of clean and dry air mass and unstable boundary layers working with the effective near-surface horizontal divergence or pumping action at the top of the boundary layer will benefit for the horizontal or vertical diffusion of surface air pollutants. However, the co-occurrence of a stable boundary layer, frequent air stagnation, positive water vapor advection and deep near-surface horizontal convergence exacerbates the air pollution.

Except for the atmospheric circulation characteristic of CTs, the durations of each circulation type also have a great influence on the local air quality. The one-day favorable or less than two-day unfavorable circulations have no significant effects on the diffusion and accumulation of air pollutants. Comparatively speaking, favorable CTs lasting for 2~4 days are beneficial for the diffusion of air pollutants, and the 3~7 days of unfavorable circulation events exacerbate the accumulation of air pollutants. The occurrences of 2~4 days of favorable and 3~7 days of unfavorable circulation are used to evaluate the atmospheric diffusion ability, which shows better diffusion abilities in 2014 and 2017 than in the other years. Taking the decrease of $PM_{2.5}$ concentration between 2016 and 2017 as an example, 59.9% of the decreased concentration over the BTH region could be attributed to the improvement in atmospheric diffusion conditions of 2017. The variation in meteorological conditions plays an important role in the interannual variation in air pollutant concentrations. The 2020 is the key and target year for the three-year action to win the battle for a blue sky goal set in 2018. It is essential to exclude the contribution of meteorological conditions to the variation in interannual air pollutants when making a quantitative evaluation of emission reduction measurements.

The quantitative evaluation of meteorological elements contribution to the interannual variation of $PM_{2.5}$ concentrations between winters of 2016 and 2017 is derived from the WRF-Chem simulation in this study. Although the model performance for $PM_{2.5}$ is generally satisfactory in Fig. S7, it shows obvious underestimation in the severe haze days. Reasons for these biases might be the overestimation in surface wind speed, uncertainties of emission inventory and insufficient treatments of some new chemistry mechanisms of particle formation, which need be further discussed in the future. In addition, some emission modules are turned off to reduce the computation cost, i.e., dust, sea salt, dimethyl sulphide, biomass burning and wildfires, which would result in the uncertainty of simulated $PM_{2.5}$ mass concentrations.

Acknowledgments: This study was supported by the National Natural Science Foundation of China (41790470 and 41805117).

Code/Data availability: The release version 4.0 of WRF-Chem can be download from http://www2.mmm.ucar.edu/wrf/users/download/get_source.html. Hourly $PM_{2.5}$ concentration observations were obtained from the website of Ministry of Ecology and Environment of the People's Republic of China (http://106.37.208.233:20035). Daily four times ECMWF ERA5 dataset during 2013 to 2018 are downloaded from https://www.ecmwf.int/en/forecasts/datasets/reanalysis-datasets/era5. Hourly observations of meteorological variables used for the WRF-Chem simulation evaluations are downloaded from the Intergrated Surface Database of National Climate Data Center (https://www.ncdc.noaa.gov/isd).

Competing interests: The authors declare that they have no conflict of interest.

Author contributions: Wang X. and Zhang R. designed research; Wang X. performed the analyses and wrote the paper; All authors contributed to the final version of the paper.

Figure Captions：

Figure 1. Interannual variation in the wintertime $PM_{2.5}$ concentrations at 114 stations over the BTH region. In each box, the central mark indicates the median, and the bottom and top edges of the box indicate the 25th and 75th percentiles, respectively. The whiskers extending to the most extreme data points are considered outliers. The region covered by the blue box in Fig. 2 is considered as the BTH region (113º-117.5ºE and 36º-42ºN).

Figure 2. The distribution of sea level pressure (shaded, unit: pa) and 10 m wind fields (vector, unit: m/s) in each circulation type. The number over each subplot indicates the occurrence frequency of the specific circulation type. The solid blue box is the location of BTH region. The daily mean geopotential height fields at 925, 850 and 500 hPa over the dashed blue box (105º-125ºE and 30º-55ºN) were applied to T-mode PCA method with the cost733 toolbox. The region mean wind speed of each circulation type is shown in Table 2.

Figure 3. The distribution of sea level pressure (unit: pa) and 10 m wind fields (unit: m/s) anomaly in each circulation type. The anomaly values are with respect to the 1980-2010 mean. Regional mean wind speed anomaly of each circulation type is summarized in Table 2.

Figure 4. The distribution of relative humidity in each circulation type (unit: %). The anomaly values are with respect to the 1980-2010 mean.

Figure 5. Zonal profile of temperature lapse rate over the BTH region (36º-42ºN) (unit: K/100 m). The gray region indicates the average altitude over 36º-42ºN. The region between the two dashed lines is the horizontal location of the BTH region (113º-117.5ºE).

Figure 6. Zonal vertical profile of vertical velocity anomaly over BTH region (unit: pa/s). The anomaly of the vertical velocities is with respect to the 1980 to 2010 mean value.

Figure 7. The box plot of the $PM_{2.5}$ concentrations varies with the circulation types. To exclude the effect of emission reduction on the annual mean $PM_{2.5}$ concentrations, the $PM_{2.5}$ distributions at the year and multiyear (average) scales are shown here, respectively. The dashed line for each year indicates the median $PM_{2.5}$ concentrations in wintertime of a specific year.

Figure 8. The daily $PM_{2.5}$ concentration anomalies vary with favorable (F) and unfavorable (U) event durations. The occurrences of CT1 and CT2 are collectively called favorable events, and CT3 to CT6 are referred to as unfavorable events. U1 indicates an unfavorable circulation event lasting for one day, and U2 means a two-day event. The central red line in each box indicates the median, and the circle is the mean value.

Figure 9. Occurrence frequencies of the effective favorable and unfavorable events. The effective favorable events referred to the favorable events lasting for two to four days. The effective unfavorable events indicate the unfavorable

events lasting for three to seven days. The specific number of days for favorable/unfavorable events is shown on the top of each bar.

Figure 10. Distributions of the observed and simulated $PM_{2.5}$ difference between the winters of 2016 and 2017. The left panel is the absolute value (unit: $\mu g/m^3$) and the right panel is the relative difference with respect to the mean value of 2016 (unit: %). The simulated seasonal mean $PM_{2.5}$ concentrations during the two years are shown in Fig. S8.

Table 1. The seasonal mean and median $PM_{2.5}$ concentrations in each atmospheric circulation type (CT) over the BTH region. $PM_{2.5}$ concentrations in bold represent the mean/median value of each CT lower than the all-case seasonal mean/median value.

Seasonal Mean/ Median ($\mu g/m^3$)	CT1	CT2	CT3	CT4	CT5	CT6
2013 (123.97/97.23)	**104.99/71.42**	**94.51/69.33**	144.76/118.50	135.47/117.20	166.28/156.52	**67.90/47.21**
2014 (93.07/75.79)	**71.03/51.52**	122.99/109.37	105.91/96.82	**86.26/72.06**	115.37/94.69	118.16/110.17
2015 (95.67/65.97)	**58.56/38**	**89.38**/73.07	134.77/114.69	135.91/106.36	124.15/99.81	106.14/70.63
2016 (112.94/91.32)	**84.74/66.16**	**110.02/88.10**	138.96/114.26	122.86/95.02	142.52/128.77	132.95/129.52
2017 (70.44/54.07)	**56.49/43.16**	**60.70/39.61**	80.03/67.39	83.89/67.24	93.63/79.28	**69.77/52.23**
2018 (79.85/63.02)	**77.99/60.68**	**51.77/37.43**	89.26/77.57	86.70/81.35	**75.08/52.72**	108.60/93.02
AVERAGE (95.27/72.22)	**73.14/53.04**	**79.12/54.89**	115.18/96.29	109.85/88.25	116.04/89.04	100.40/82.04

Table 2. Regional mean meteorological variables over the BTH region under each circulation type

Variables	CT1	CT2	CT3	CT4	CT5	CT6
Surface wind speed (m/s)	3.27	2.31	2.71	2.24	2.58	2.54
Surface wind speed anomaly (m/s)	0.53	-0.42	-0.04	-0.49	-0.15	-0.19
Mean vertical velocity anomaly between 850 to 1000 hPa (pa/s)	0.04	-0.0358	-0.0038	-0.0296	-0.0111	-0.0213
Difference of temperature anomaly between 850 and 1000 hPa (K)	-0.716	-0.206	0.664	0.456	0.232	0.485

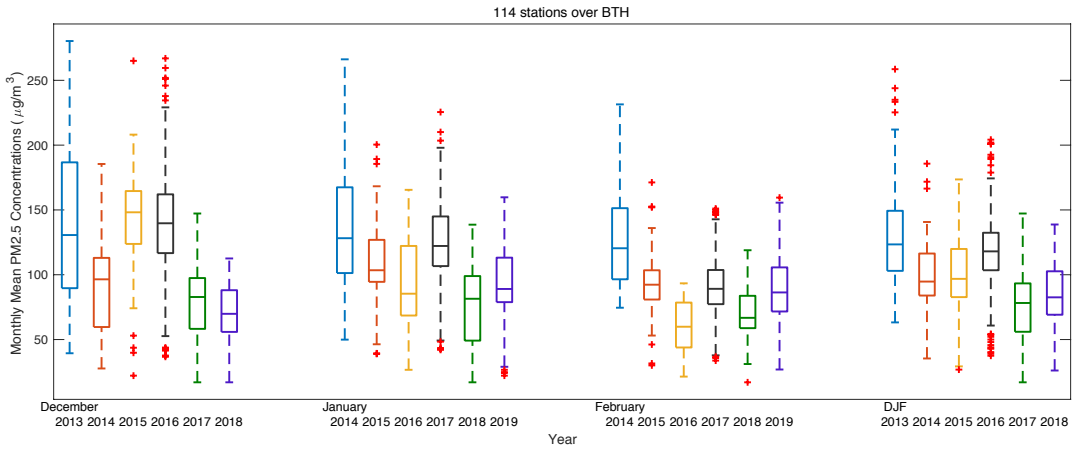

501

502 Figure 1. Interannual variation in the wintertime $PM_{2.5}$ concentrations at 114 stations over the BTH region. In each
503 box, the central mark indicates the median, and the bottom and top edges of the box indicate the 25th and 75th
504 percentiles, respectively. The whiskers extending to the most extreme data points are considered outliers. The region
505 covered by the blue box in Fig. 2 is considered as the BTH region (113º-117.5ºE and 36º-42ºN).

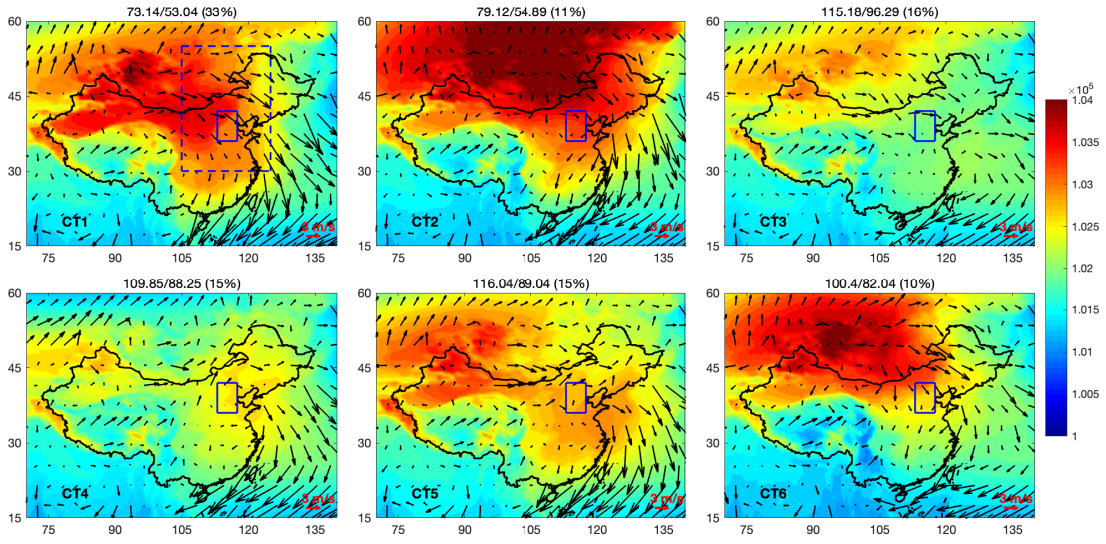

506

507 Figure 2. The distribution of sea level pressure (shaded, unit: pa) and 10 m wind fields (vector, unit: m/s) in each
508 circulation type. The number over each subplot indicates the occurrence frequency of the specific circulation type.
509 The solid blue box is the location of BTH region. The daily mean geopotential height fields at 925, 850 and 500 hPa
510 over the dashed blue box (105º-125ºE and 30º-55ºN) were applied to T-mode PCA method with the cost733 toolbox.
511 The region mean wind speed of each circulation type is shown in Table 2.

512

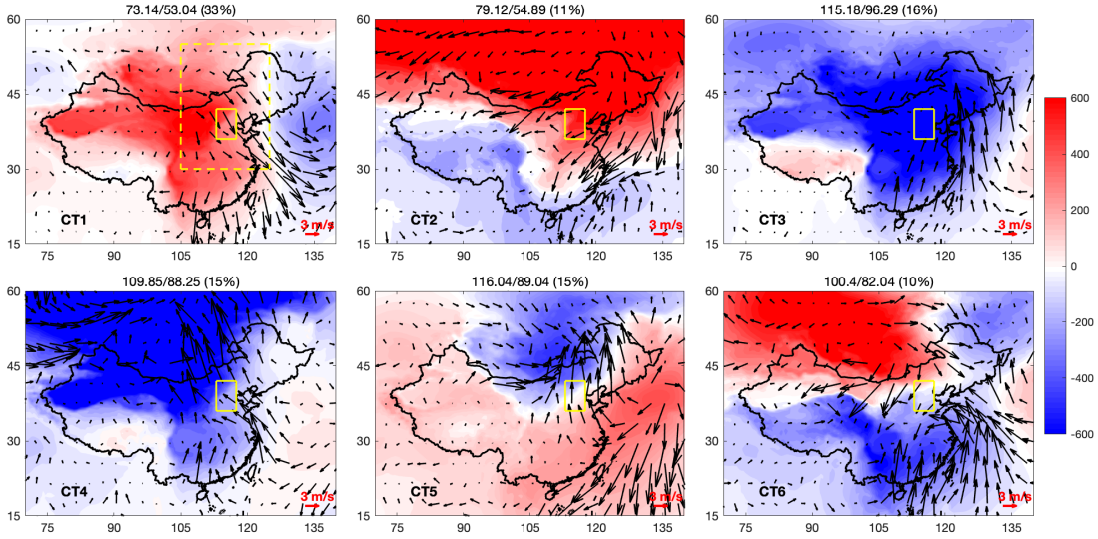

513

514 Figure 3. The distribution of sea level pressure (unit: pa) and 10 m wind fields (unit: m/s) anomaly in each circulation
515 type. The anomaly values are with respect to the 1980-2010 mean. Regional mean wind speed anomaly of each
516 circulation type is summarized in Table 2.

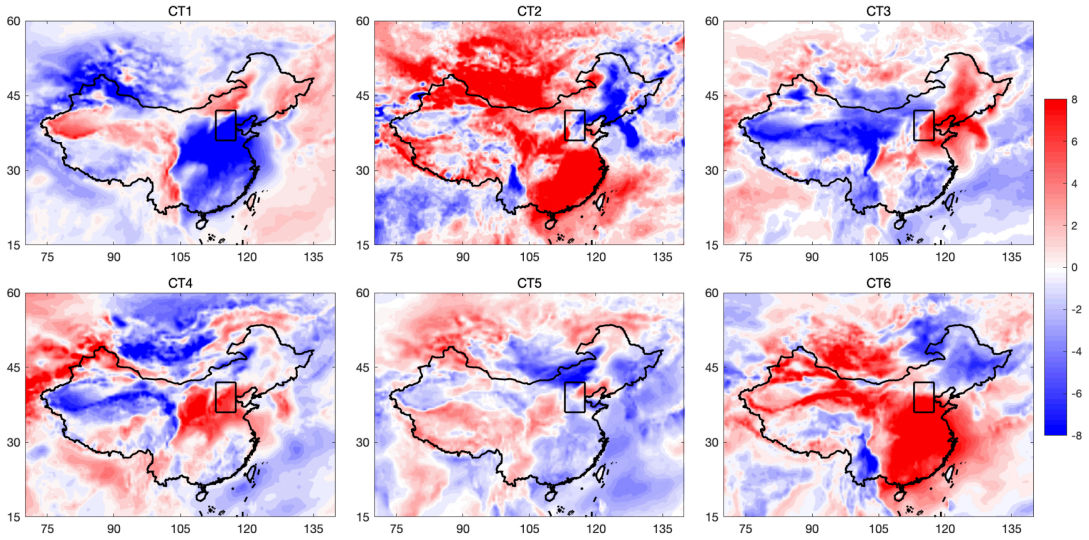

517

518 Figure 4. The distribution of relative humidity in each circulation type (unit: %). The anomaly values are with respect
519 to the 1980-2010 mean.

520

521

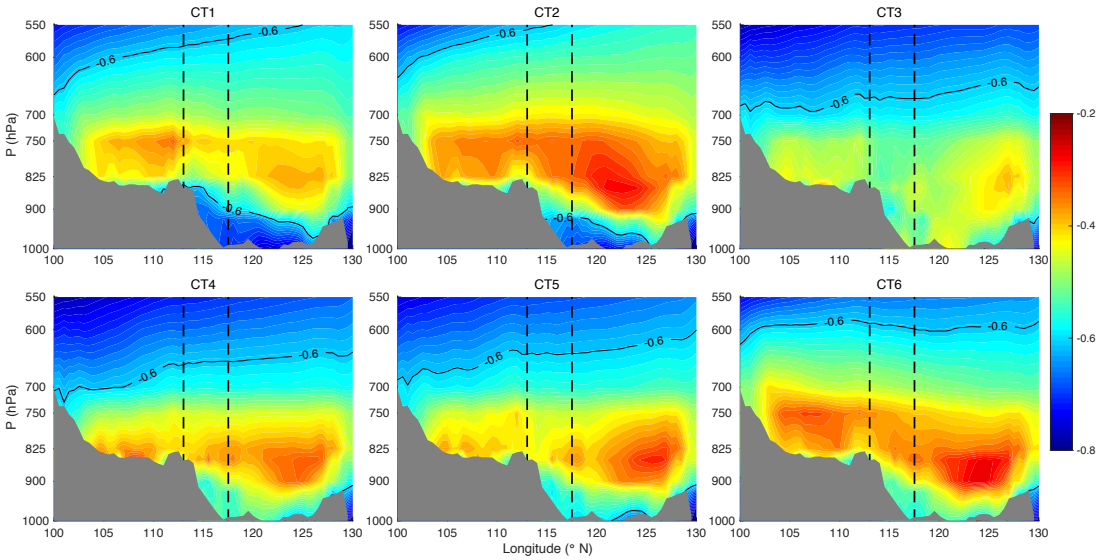

522

523 Figure 5. Zonal profile of temperature lapse rate over the BTH region (36º-42ºN) (unit: K/100 m). The gray region
524 indicates the average altitude over 36º-42ºN. The region between the two dashed lines is the horizontal location of
525 the BTH region (113º-117.5ºE).

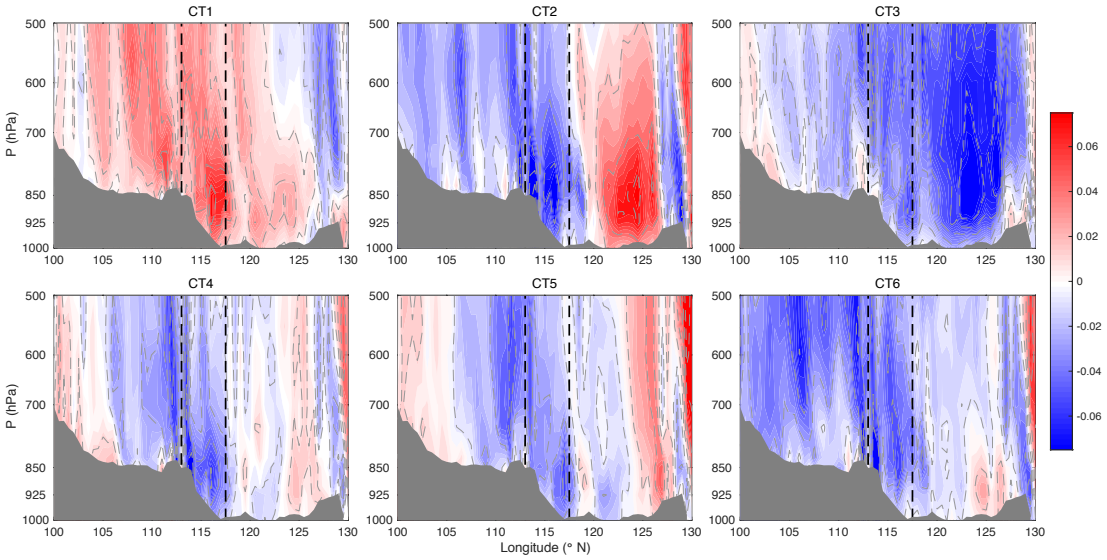

526

527 Figure 6. Zonal vertical profile of vertical velocity anomaly over BTH region (unit: pa/s). The anomaly of the vertical
528 velocities is with respect to the 1980 to 2010 mean value.

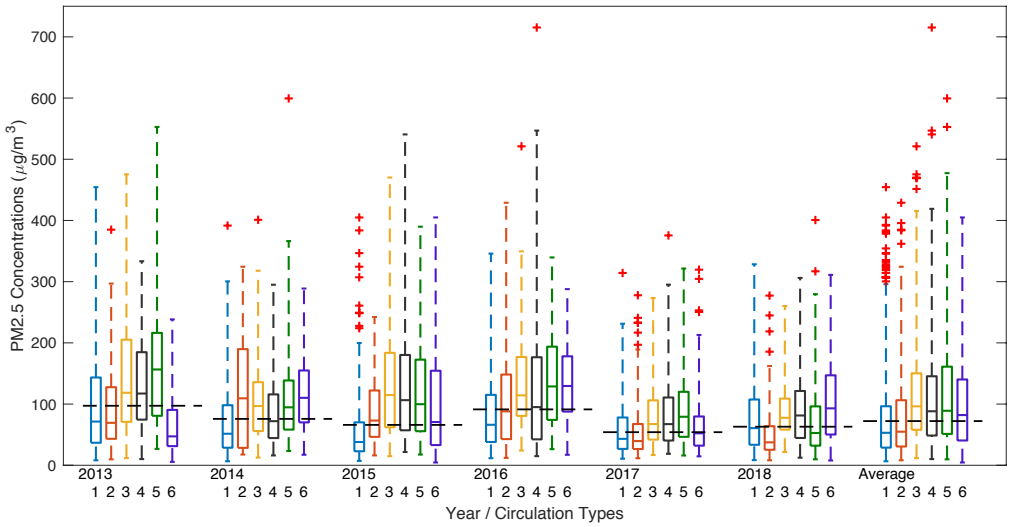

529

530 Figure 7. The box plot of the $PM_{2.5}$ concentrations varies with the circulation types. To exclude the effect of emission
531 reduction on the annual mean $PM_{2.5}$ concentrations, the $PM_{2.5}$ distributions at the year and multiyear (average) scales
532 are shown here, respectively. The dashed line for each year indicates the median $PM_{2.5}$ concentrations in wintertime
533 of a specific year.

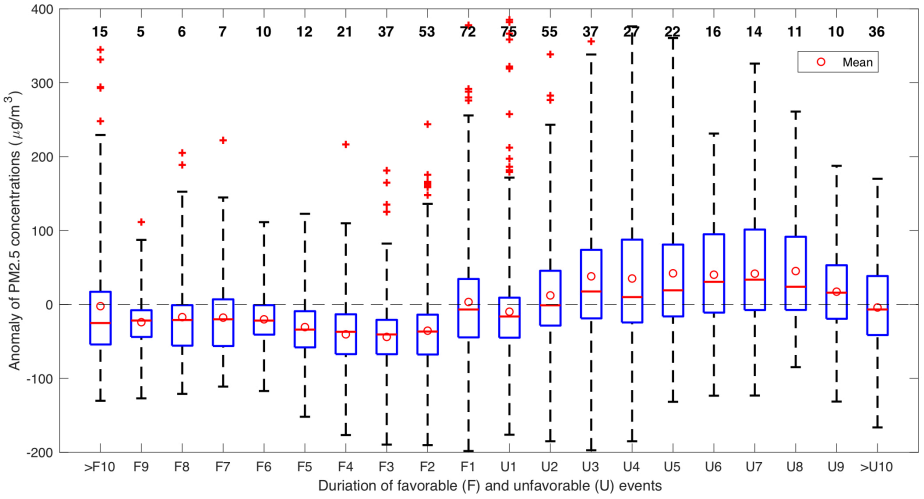

534

535 Figure 8. The daily $PM_{2.5}$ concentration anomalies vary with favorable (F) and unfavorable (U) event durations. The
536 occurrences of CT1 and CT2 are collectively called favorable events, and CT3 to CT6 are referred to as unfavorable
537 events. U1 indicates an unfavorable circulation event lasting for one day, and U2 means a two-day event. The central
538 red line in each box indicates the median, and the circle is the mean value.

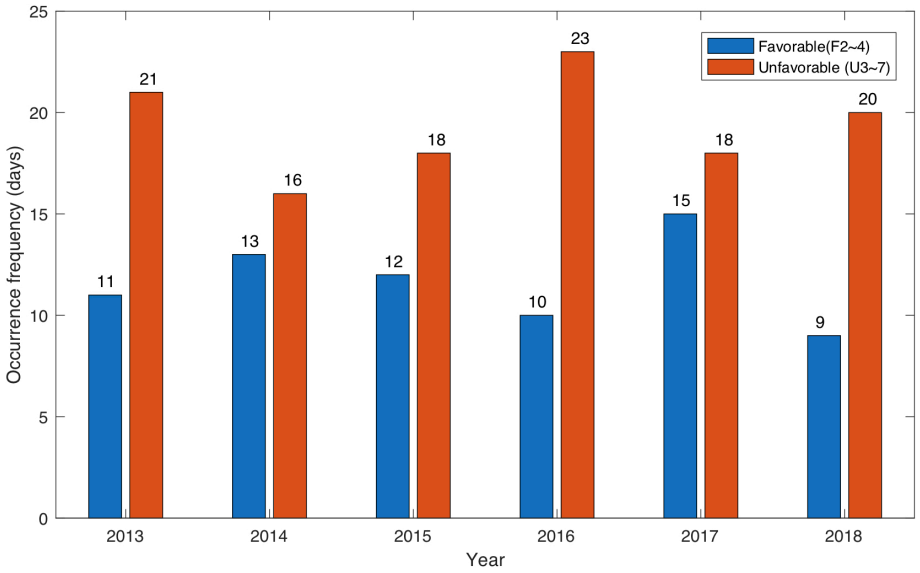

539

540 Figure 9. Occurrence frequencies of the effective favorable and unfavorable events. The effective favorable events
541 referred to the favorable events lasting for two to four days. The effective unfavorable events indicate the unfavorable
542 events lasting for three to seven days. The specific number of days for favorable/unfavorable events is shown on the
543 top of each bar.

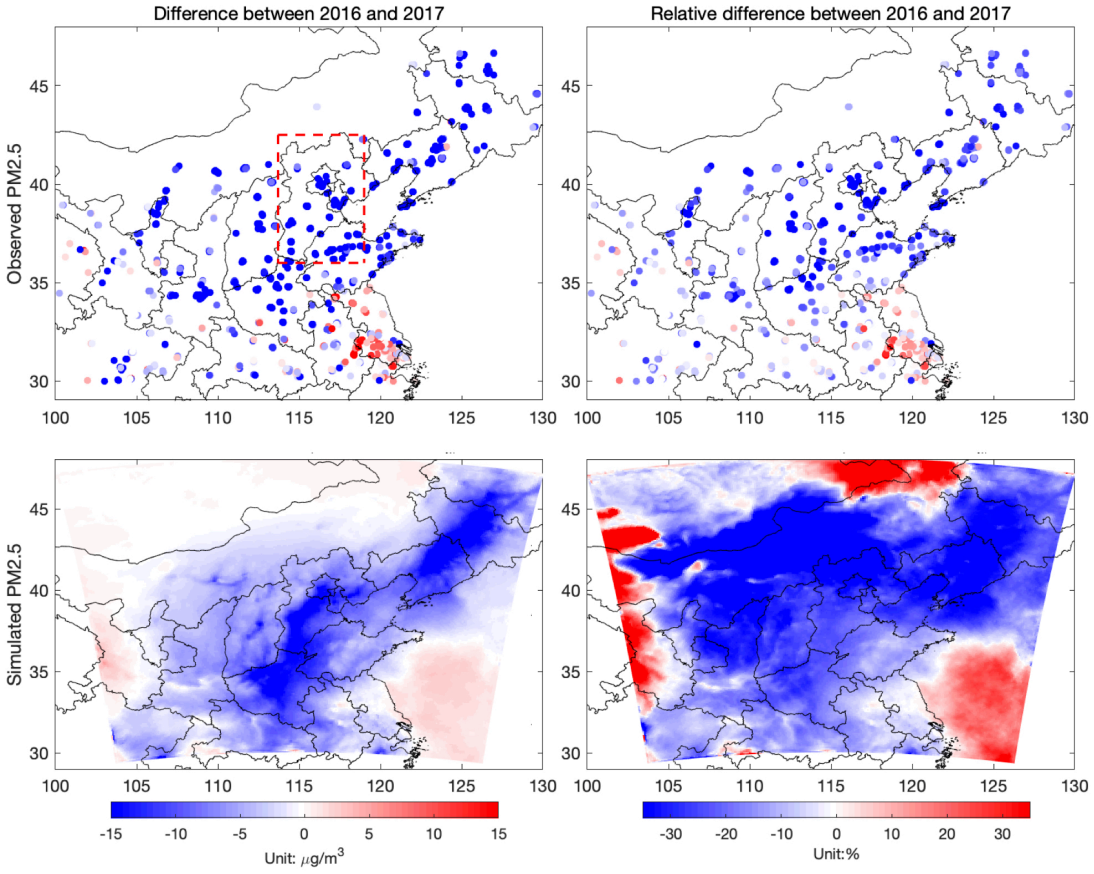

544

545 Figure 10. Distributions of the observed and simulated $PM_{2.5}$ difference between the winters of 2016 and 2017. The

left panel is the absolute value (unit: $\mu g/m^3$) and the right panel is the relative difference with respect to the mean value of 2016 (unit: %). The simulated seasonal mean $PM_{2.5}$ concentrations during the two years are shown in Fig. S8.

Reference:

Ackermann, I. J., Hass, H., Memmesheimer, M., Ebel, A., Binkowski, F. S., and Shankar, U.: Modal aerosol dynamics model for Europe: Development and first applications, Atmos. Environ., 32, 2981-2999, 1998.

Bi, J., Huang, J., Holben, B. N., and Zhang, G.: Comparison of Key Absorption and Optical Properties Between Pure and Transported Anthropogenic Dust over East and Central Asia, Atmos. Chem. Phys., 16, 15501-15516, 2016.

Cai, W., Li, K., Liao, H., Wang, H., and Wu, L. J. N. C. C.: Weather conditions conducive to Beijing severe haze more frequent under climate change, 7, 257-262, 2017.

Cavazos, T.: Using self-organizing maps to investigate extreme climate events: An application to wintertime precipitation in the Balkans, J. Climate, 13, 1718-1732, 2000.

Che, H., Xia, X., Zhao, H., Dubovik, O., Holben, B. N., Goloub, P., Cuevas-Agulló, E., Estelles, V., Wang, Y., and Zhu, J.: Spatial distribution of aerosol microphysical and optical properties and direct radiative effect from the China Aerosol Remote Sensing Network, Atmos. Chem. Phys., 19, 11843-11864, 2019.

Chen, H., and Wang, H.: Haze Days in North China and the associated atmospheric circulations based on daily visibility data from 1960 to 2012, Journal of Geophysical Research, 120, 5895-5909, 2015.

Chen, H., Wang, H., Sun, J., Xu, Y., and Yin, Z.: Anthropogenic fine particulate matter pollution will be exacerbated in eastern China due to 21st century GHG warming, Atmos. Chem. Phys., 19, 233-243, 2019a.

Chen, S., Zhang, X., Lin, J., Huang, J., Zhao, D., Yuan, T., Huang, K., Luo, Y., Jia, Z., and Zang, Z.: Fugitive Road Dust PM2.5 Emissions and Their Potential Health Impacts, Environ. Sci. Technol., 53, 8455-8465, 2019b.

Chen, Y., Zhao, C., and Ming, Y.: Potential impacts of Arctic warming on Northern Hemisphere mid-latitude aerosol optical depth, Clim. Dynam., 53, 1637-1651, 2019c.

Chen, Z., Chen, D., Kwan, M.-P., Chen, B., Gao, B., Zhuang, Y., Li, R., and Xu, B.: The control of anthropogenic emissions contributed to 80% of the decrease in PM 2.5 concentrations in Beijing from 2013 to 2017, Atmos. Chem. Phys., 19, 13519-13533, 2019d.

Notice of the General Office of the State Council on Issuing the Air Pollution Prevention and Control Action Plan: http://www.gov.cn/zwgk/2013-09/12/ content_2486773.htm, access: 30/12/2019, 2013.

The State Council rolls out a three-year action plan for clean air: http://www.gov.cn/zhengce/content/2018-07/03/content_5303158.htm, access: 30/12/2019, 2018.

Collins, W. D., Rasch, P. J., Boville, B. A., Hack, J. J., McCaa, J. R., Williamson, D. L., Kiehl, J. T., Briegleb, B., Bitz, C., and Lin, S.-J.: Description of the NCAR community atmosphere model (CAM 3.0), NCAR Tech. Note NCAR/TN-464+ STR, 226, 2004.

Dang, R., and Liao, H.: Severe winter haze days in the Beijing–Tianjin–Hebei region from 1985 to 2017 and the roles of anthropogenic emissions and meteorology, Atmos. Chem. Phys., 19, 10801-10816, 2019.

Ding, A., Huang, X., Nie, W., Chi, X., Xu, Z., Zheng, L., Xu, Z., Xie, Y., Qi, X., Shen, Y., Sun, P., Wang, J., Wang,

L., Sun, J., Yang, X. Q., Qin, W., Zhang, X., Cheng, W., Liu, W., Pan, L., and Fu, C.: Significant reduction of PM2.5 in eastern China due to regional-scale emission control: evidence from SORPES in 2011–2018, Atmos. Chem. Phys., 19, 11791-11801, 10.5194/acp-19-11791-2019, 2019.

Fan, H., Zhao, C., and Yang, Y.: A comprehensive analysis of the spatio-temporal variation of urban air pollution in China during 2014–2018, Atmos. Environ., 220, 117066, 2020.

Feng, F., and Wang, K.: Determining Factors of Monthly to Decadal Variability in Surface Solar Radiation in China: Evidences From Current Reanalyses, Journal of Geophysical Research, 124, 9161-9182, 2019.

Feng, J., Li, J., Liao, H., and Zhu, J.: Simulated coordinated impacts of the previous autumn North Atlantic Oscillation (NAO) and winter El Niño on winter aerosol concentrations over eastern China, Atmos. Chem. Phys., 19, 10787-10800, 2019.

Garrett, T. J., Zhao, C., and Novelli, P. C.: Assessing the relative contributions of transport efficiency and scavenging to seasonal variability in Arctic aerosol, Tellus B, 62, 190-196, 2010.

Gui, K., Che, H., Wang, Y., Wang, H., Zhang, L., Zhao, H., Zheng, Y., Sun, T., and Zhang, X.: Satellite-derived PM2. 5 concentration trends over Eastern China from 1998 to 2016: Relationships to emissions and meteorological parameters, Environ. Pollut., 247, 1125-1133, 2019.

Guo, J., Xu, H., Liu, L., Chen, D., Peng, Y., Yim, S. H. L., Yang, Y., Li, J., Zhao, C., and Zhai, P.: The trend reversal of dust aerosol over East Asia and the North Pacific Ocean attributed to large-scale meteorology, deposition and soil moisture, J. Geophys. Res: Atmos., 2019.

He, J., Lu, S., Yu, Y., Gong, S., Zhao, S., and Zhou, C.: Numerical Simulation Study of Winter Pollutant Transport Characteristics over Lanzhou City, Northwest China, Atmosphere, 9, 382, 2018a.

He, Y., Wang, K., Zhou, C., and Wild, M.: A Revisit of Global Dimming and Brightening Based on the Sunshine Duration, Geophys. Res. Lett., 45, 4281-4289, 2018b.

Hong, C., Zhang, Q., Zhang, Y., Davis, S. J., Tong, D., Zheng, Y., Liu, Z., Guan, D., He, K., and Schellnhuber, H. J.: Impacts of climate change on future air quality and human health in China, P. Natl. Acad. Sci., 116, 17193-17200, 2019.

Hu, Z., Huang, J., Zhao, C., Ma, Y., Jin, Q., Qian, Y., Leung, L. R., Bi, J., and Ma, J.: Trans-Pacific transport and evolution of aerosols: spatiotemporal characteristics and source contributions, Atmos. Chem. Phys., 19, 12709-12730, 2019.

Huang, X., Wang, Z., and Ding, A.: Impact of Aerosol-PBL Interaction on Haze Pollution: Multiyear Observational Evidences in North China, Geophys. Res. Lett., 45, 8596-8603, 2018.

Huth, R.: A circulation classification scheme applicable in GCM studies, Theor. Appl. Climatol., 67, 1-18, 2000.

Huth, R., Beck, C., Philipp, A., Demuzere, M., Ustrnul, Z., Cahynová, M., Kyselý, J., and Tveito, O. E.: Classifications of atmospheric circulation patterns: recent advances and applications, Ann. NY AcaD. Sci., 1146, 105-152, 2008.

Iacono, M. J., Delamere, J. S., Mlawer, E. J., Shephard, M. W., Clough, S. A., and Collins, W. D.: Radiative forcing by long-lived greenhouse gases: Calculations with the AER radiative transfer models, Journal of Geophysical

Research: Atmospheres, 113, 2008.

Janjić, Z. I.: The Step-Mountain Eta Coordinate Model: Further Developments of the Convection, Viscous Sublayer, and Turbulence Closure Schemes, Monthly Weather Review, 122, 927-945, 10.1175/1520-0493(1994)122<0927:TSMECM>2.0.CO;2, 1994.

Jian, B., Li, J., Wang, G., He, Y., Han, Y., Zhang, M., and Huang, J.: The Impacts of Atmospheric and Surface Parameters on Long-Term Variations in the Planetary Albedo, J. Climate, 31, 8705-8718, 2018.

Leung, D. M., Tai, A. P., Mickley, L. J., Moch, J. M., Donkelaar, A. v., Shen, L., and Martin, R. V.: Synoptic meteorological modes of variability for fine particulate matter (PM 2.5) air quality in major metropolitan regions of China, Atmos. Chem. Phys., 18, 6733-6748, 2018.

Li, G., Zavala, M., Lei, W., Tsimpidi, A., Karydis, V., Pandis, S. N., Canagaratna, M., and Molina, L.: Simulations of organic aerosol concentrations in Mexico City using the WRF-CHEM model during the MCMA-2006/MILAGRO campaign, Atmos. Chem. Phys., 11, 3789-3809, 2011.

Li, J., Lv, Q., Jian, B., Zhang, M., Zhao, C., Fu, Q., Kawamoto, K., and Zhang, H.: The impact of atmospheric stability and wind shear on vertical cloud overlap over the Tibetan Plateau, Atmos. Chem. Phys., 18, 7329-7343, 2018.

Li, J., Liao, H., Hu, J., and Li, N.: Severe particulate pollution days in China during 2013–2018 and the associated typical weather patterns in Beijing-Tianjin-Hebei and the Yangtze River Delta regions, Environ. Pollut., 248, 74-81, 2019.

Li, Q., Zhang, R., and Wang, Y.: Interannual variation of the wintertime fog–haze days across central and eastern China and its relation with East Asian winter monsoon, Int. J. Climatol., 36, 346-354, 2016.

Liu, C., Chen, R., Sera, F., Vicedo-Cabrera, A. M., Guo, Y., Tong, S., Coelho, M. S., Saldiva, P. H., Lavigne, E., and Matus, P.: Ambient particulate air pollution and daily mortality in 652 cities, New Engl. J. Med., 381, 705-715, 2019.

Miao, Y., Guo, J., Liu, S., Liu, H., Li, Z., Zhang, W., and Zhai, P.: Classification of summertime synoptic patterns in Beijing and their associations with boundary layer structure affecting aerosol pollution, Atmos. Chem. Phys., 17, 3097-3110, 2017.

Mu, M., and Zhang, R. J. S. C. E. S.: Addressing the issue of fog and haze: A promising perspective from meteorological science and technology, 57, 1, 2014.

Philipp, A., Beck, C., Esteban, P., Kreienkamp, F., Krennert, T., Lochbihler, K., Lykoudis, S. P., Pianko-Kluczynska, K., Post, P., and Alvarez10, D. R.: cost733class-1.2 User guide, Augsburg, Germany, 10-21, 2014.

Schell, B., Ackermann, I. J., Hass, H., Binkowski, F. S., and Ebel, A.: Modeling the formation of secondary organic aerosol within a comprehensive air quality model system, J. Geophys. Res: Atmos., 106, 28275-28293, 2001.

Song, Z., Fu, D., Zhang, X., Wu, Y., Xia, X., He, J., Han, X., Zhang, R., and Che, H.: Diurnal and seasonal variability of PM2. 5 and AOD in North China plain: Comparison of MERRA-2 products and ground measurements, Atmos. Environ., 191, 70-78, 2018.

Stockwell, W. R., Middleton, P., Chang, J. S., and Tang, X.: The second generation regional acid deposition model chemical mechanism for regional air quality modeling, J. Geophys. Res: Atmos., 95, 16343-16367, 1990.

Sun, Y., Zhao, C., Su, Y., Ma, Z., Li, J., Letu, H., Yang, Y., and Fan, H.: Distinct Impacts of Light and Heavy Precipitation on PM2.5 Mass Concentration in Beijing, Earth Space Sci., 6, 1915-1925, 2019.

Tao, S., Ru, M. Y., Du, W., Zhu, X., Zhong, Q. R., Li, B. G., Shen, G. F., Pan, X. L., Meng, W. J., Chen, Y. L., Shen, H. Z., Lin, N., Su, S., Zhuo, S. J., Huang, T. B., Xu, Y., Yun, X., Liu, J. F., Wang, X. L., Liu, W. X., Cheng, H. F., and Zhu, D. Q.: Quantifying the rural residential energy transition in China from 1992 to 2012 through a representative national survey, Nature Energy, 3, 567-573, 10.1038/s41560-018-0158-4, 2018.

Tie, X., Zhang, Q., He, H., Cao, J., Han, S., Gao, Y., Li, X., and Jia, X. C.: A budget analysis of the formation of haze in Beijing, Atmos. Environ., 100, 25-36, 2015.

Valverde, V., Pay, M. T., and Baldasano, J. M.: Circulation-type classification derived on a climatic basis to study air quality dynamics over the Iberian Peninsula, Int. J. Climatol., 35, 2877-2897, 2015.

Wang, H., Chen, H., and Liu, J.: Arctic Sea Ice Decline Intensified Haze Pollution in Eastern China, Atmos. Ocean. Sci. Lett., 8, 1-9, 2015.

Wang, K., Dickinson, R. E., and Liang, S.: Clear sky visibility has decreased over land globally from 1973 to 2007, Science, 323, 1468-1470, 2009.

Wang, X., and Wang, K.: Homogenized Variability of Radiosonde-Derived Atmospheric Boundary Layer Height over the Global Land Surface from 1973 to 2014, J. Climate, 29, 6893-6908, 2016.

Wang, X., Wang, K., and Su, L.: Contribution of atmospheric diffusion conditions to the recent improvement in air quality in China, Sci. Rep., 6, 36404, 2016.

Wang, X., Wen, H., Shi, J., Bi, J., Huang, Z., Zhang, B., Zhou, T., Fu, K., Chen, Q., and Xin, J.: Optical and microphysical properties of natural mineral dust and anthropogenic soil dust near dust source regions over northwestern China, Atmos. Chem. Phys., 18, 2119-2138, 2017.

Wang, X., Dickinson, R. E., Su, L., Zhou, C., and Wang, K.: PM2. 5 pollution in China and how it has been exacerbated by terrain and meteorological conditions, B. Am. Meteorol. Soc., 99, 105-119, 2018.

Wang, X., Zhang, R., and Yu, W. J. J. o. G. R. A.: The effects of PM2. 5 concentrations and relative humidity on atmospheric visibility in Beijing, 124, 2235-2259, 2019a.

Wang, Y., Li, W., Gao, W., Liu, Z., Tian, S., Shen, R., Ji, D., Wang, S., Wang, L., and Tang, G.: Trends in particulate matter and its chemical compositions in China from 2013–2017, Sci. China Earth Sci., 1-15, 2019b.

Xu, J., Chang, L., Qu, Y., Yan, F., Wang, F., and Fu, Q.: The meteorological modulation on PM2. 5 interannual oscillation during 2013 to 2015 in Shanghai, China, Sci. Total Environ., 572, 1138-1149, 2016.

Yang, X., Zhao, C., Zhou, L., Li, Z., Cribb, M., and Yang, S.: Wintertime cooling and a potential connection with transported aerosols in Hong Kong during recent decades, Atmos. Res., 211, 52-61, 10.1016/J.ATMOSRES.2018.04.029, 2018.

Yin, Z., Wang, H., and Chen, H.: Understanding severe winter haze events in the North China Plain in 2014: roles of climate anomalies, Atmos. Chem. Phys., 17, 1641-1651, 2017.

Yin, Z., Wang, H., and Ma, X.: Possible Relationship between the Chukchi Sea Ice in the Early Winter and the February Haze Pollution in the North China Plain, J. Climate, 32, 5179-5190, 2019.

Zhai, S., Jacob, D. J., Wang, X., Shen, L., Li, K., Zhang, Y., Gui, K., Zhao, T., and Liao, H.: Fine particulate matter (PM2.5) trends in China, 2013–2018: separating contributions from anthropogenic emissions and meteorology, Atmos. Chem. Phys., 19, 11031-11041, 10.5194/acp-19-11031-2019, 2019.

Zhang, J. P., Zhu, T., Zhang, Q., Li, C., Shu, H., Ying, Y., Dai, Z., Wang, X., Liu, X., and Liang, A.: The impact of circulation patterns on regional transport pathways and air quality over Beijing and its surroundings, Atmos. Chem. Phys., 12, 5031-5053, 2012.

Zhang, K., Zhao, C., Fan, H., Yang, Y., and Sun, Y.: Toward Understanding the Differences of PM 2.5 Characteristics Among Five China Urban Cities, Asia Pac. J. Atmos. Sci., 1-10, 10.1007/S13143-019-00125-W, 2019a.

Zhang, Q., Jiang, X., Tong, D., Davis, S. J., Zhao, H., Geng, G., Feng, T., Zheng, B., Lu, Z., and Streets, D. G.: Transboundary health impacts of transported global air pollution and international trade, Nature, 543, 705, 2017.

Zhang, Q., and Geng, G.: Impact of clean air action on PM 2.5 pollution in China, in, Springer, 2019.

Zhang, Q., Zheng, Y., Tong, D., Shao, M., Wang, S., Zhang, Y., Xu, X., Wang, J., He, H., and Liu, W.: Drivers of improved PM2. 5 air quality in China from 2013 to 2017, P. Natl. Acad. Sci., 116, 24463-24469, 2019b.

Zhang, Q., Song, Y., Li, M., and Zheng, B.: Anthropogenic Emissions of SO2, NOx, and NH3 in China, in: Atmospheric Reactive Nitrogen in China: Emission, Deposition and Environmental Impacts, edited by: Liu, X., and Du, E., Springer Singapore, Singapore, 13-40, 2020.

Zhang, R., Li, Q., and Zhang, R.: Meteorological conditions for the persistent severe fog and haze event over eastern China in January 2013, Sci. China Earth Sci., 57, 26-35, 2014.

Zhang, R. J. N. C. C.: Atmospheric science: Warming boosts air pollution, 7, 238-239, 2017.

Zhang, X., Xu, X., Ding, Y., Liu, Y., Zhang, H., Wang, Y., and Zhong, J.: The impact of meteorological changes from 2013 to 2017 on PM 2.5 mass reduction in key regions in China, Sci. China Earth Sci., 1-18, 2019c.

Zhang, Y., Vu, V. T., Sun, J., He, J., Shen, X., Lin, W., Zhang, X., Zhong, J., Gao, W., and Wang, Y.: Significant changes in chemistry of fine particles in wintertime Beijing from 2007 to 2017: Impact of clean air actions, Environ. Sci. Technol., 2019d.

Zhao, B., Zheng, H., Wang, S., Smith, K. R., Lu, X., Aunan, K., Gu, Y., Wang, Y., Ding, D., and Xing, J.: Change in household fuels dominates the decrease in PM2. 5 exposure and premature mortality in China in 2005–2015, P. Natl. Acad. Sci., 115, 12401-12406, 2018a.

Zhao, C., and Garrett, T. J.: Effects of Arctic haze on surface cloud radiative forcing, Geophys. Res. Lett., 42, 557-564, 10.1002/2014GL062015, 2015.

Zhao, C., Yanan, L. I., Zhang, F., Sun, Y., and Wang, P.: Growth rates of fine aerosol particles at a site near Beijing in June 2013, Adv. Atmos. Sci., 35, 209-217, 2018b.

Zhao, C., Wang, Y., Shi, X., Zhang, D., Wang, C., Jiang, J. H., Zhang, Q., and Fan, H.: Estimating the Contribution of Local Primary Emissions to Particulate Pollution Using High-Density Station Observations, J. Geophys. Res: Atmos., 124, 1648-1661, 2019a.

Zhao, C., Yang, Y., Fan, H., Huang, J., Fu, Y., Zhang, X., Kang, S., Cong, Z., Letu, H., and Menenti, M.: Aerosol characteristics and impacts on weather and climate over the Tibetan Plateau, Natl. Sci. Rev., 10.1093/NSR/NWZ184,

2019b.

Zhao, C., Yu, Y., Kuang, Y., Tao, J., and Zhao, G.: Recent progress of aerosol light-scattering enhancement factor studies in China, Adv. Atmos. Sci., 36, 1015-1026, 2019c.

Zhao, H., Che, H., Xia, X., Wang, Y., Wang, H., Wang, P., Ma, Y., Yang, H., Liu, Y., and Wang, Y.: Multiyear Ground-Based Measurements of Aerosol Optical Properties and Direct Radiative Effect Over Different Surface Types in Northeastern China, J. Geophys. Res: Atmos., 123, 13,887-813,916, 2018c.

Zhao, S., Zhang, H., and Xie, B.: The effects of El Niño–Southern Oscillation on the winter haze pollution of China, Atmos. Chem. Phys., 18, 1863, 2018d.

Zheng, B., Tong, D., Li, M., Liu, F., Hong, C., Geng, G., Li, H., Li, X., Peng, L., and Qi, J.: Trends in China's anthropogenic emissions since 2010 as the consequence of clean air actions, Atmos. Chem. Phys., 18, 14095-14111, 2018.

Zhong, Q., Ma, J., Shen, G., Shen, H., Zhu, X., Yun, X., Meng, W., Cheng, H., Liu, J., Li, B., Wang, X., Zeng, E. Y., Guan, D., and Tao, S.: Distinguishing Emission-Associated Ambient Air PM2.5 Concentrations and Meteorological Factor-Induced Fluctuations, Environ. Sci. Technol., 52, 10416-10425, 10.1021/acs.est.8b02685, 2018.